Structural and optoelectronic properties of CdS/Y/CdS thin films

A.F. Qasrawi, Tamara Y. Abed

PII: S0040-6090(19)30210-X
DOI: https://doi.org/10.1016/j.tsf.2019.04.016
Reference: TSF 37241

To appear in: *Thin Solid Films*

Received date: 16 September 2018
Revised date: 8 April 2019
Accepted date: 8 April 2019

Please cite this article as: A.F. Qasrawi and T.Y. Abed, Structural and optoelectronic properties of CdS/Y/CdS thin films, Thin Solid Films, https://doi.org/10.1016/j.tsf.2019.04.016

Structural and optoelectronic properties of CdS/Y/CdS thin films

A. F. Qasrawi [a,c,*],Tamara Y. Abed[a]

[a] *Department of Physics, Arab American University, Jenin, Palestine*
[c] *Group of physics, Faculty of Engineering, Atilim University, 06836 Ankara, Turkey*

Abstract

In the current study, the structural, optical, photoelectrical and electrical properties of CdS/Y/CdS thin films are investigated. The current design include the evaporation of a layer of 70 nm thick yttrium between two layers of CdS. Each CdS layer is of thickness of 500 nm. It is observed that the yttrium slab increased the microstrain, defect density, stacking faults and decreased the grain size and redshifts the indirect allowed transitions energy band gap of CdS. In addition an enhancement by ~5 times in the light absorbability is detected at 1.74 eV. The enhanced absorbance results in increasing the photocurrent by ~ 21 times and changed the recombination mechanism from a trap assisted recombination to supralinear recombination mechanisms. Moreover, the ac signal analysis in the frequency domain of 10-1800 MHz has shown that the yttrium forces the CdS to exhibit negative capacitance effect and make it behave as band stop filter with notch frequency of 1520 MHz. The quality of the CdS/Y/CdS films as microwave cavities are screened by the evaluation of the return loss which revealed good features of the nanostructured films as microwave receivers.

Keywords; Cadmium sulfide; Yttrium; Tri-layer; Optical properties; Impedance spectroscopy; Photocurrent

---

*Correspond author email atef.qasrawi@atilim.edu.tr; atef.qasrawi@aauj.edu

Tel 00970599379412; fax 0097042518888

1. Introduction

Cadmium sulfide thin films are under the focus owing to their wide range of applications. They have been employed in optoelectronic technology for solar energy harvesting [1]. They also find applications as catalyst [2], memory cells [3] and as tunneling barriers [4]. CdS films combined to p-type silicon substrate are reported to exhibit high performance as solar cells. The optimized efficiency for these cells after the insertion of MoO_3 layer between cadmium sulfide film and silicon substrate reached 10.64%. For these cells, the short circuit current, the open voltage and the fill factor are reported to be 28.75 mA/cm^2, 543 mV and 68.13%, respectively, under traditional conditions [1]. In addition, a nonvolatile memory characteristic of high-*k* MOS capacitors made of cadmium sulfide embedded Zr-doped HfO_2 are reported [3]. The CdS embedded devices revealed good memory and charge retention characteristics which make it suitable for low voltage nonvolatile memory applications. Moreover, when the CdS was coated with 20 nm thick Sb_2Te_3, it shows negative differential capacitance effect in the frequency domain of 0.26 –1.8 GHz. The heterojunction device performed as low pass filters with ideal values of voltage standing wave ratios [4]. In another work, CdS thin films which are prepared onto fluorine doped tin oxide (FTO), indium tin oxide and Si wafer are observed to exhibit the best features when coated onto FTO substrates. This substrate make CdS suitable for electron-transport layer in perovskite solar cells due to its good conductivity, crystallinity and an appropriate conduction band level [5]. In addition, heat treated CdS thin films that are annealed at 500 ^oC [6, 7] are found to be appropriate for window and hole-locking layers in CdTe-based perovskite solar cells.

The above mentioned applications encouraged the research society to find methods that target improving the physical properties of CdS to make it more appropriate for technological applications. As for example, in one of our recent works we have inserted a thin metallic layer of ytterbium between two layers of CdS [8] to form the CdS (500 nm)/Yb (70 nm)/CdS (500 nm) structure. The insertion of

Yb layer improved the crystallinity of CdS and raised the absorbability of this material by 8 times. It also increased the drift mobility of CdS from 281 to 996 cm^2/Vs. The devices are found to be attractive for use as wave traps [8]. In the current work, we target to study the effects that are associated with the insertion of yttrium film of thickness of 70 nm between two layers of CdS. Particularly, the structural, compositional, morphological, optical and dielectric properties of the Y-sandwiched CdS are investigated and compared to pure CdS. In addition, the effect of the yttrium layer on the photocurrent-laser light power dependence of the CdS as well as on impedance spectral parameters are explored.

The reasons for replacing Yb by Y in the current work are the hexagonal nature of Y which is more consistent with that of hexagonal CdS and the ionic radius of Y being larger than that of Yb and Cd. Both of the CdS and yttrium has the same plane orientations. The similarity in the hexagonal crystalline nature and in the plane orientations of Y and CdS reduces the lattice mismatches between the CdS and Y compared to the cubic Yb. In addition, the ionic radius of Y^{+3} being larger than that of Cd^{+2} is expected to cause a reduction in the grain size that in turn results in larger defect density values and as a result increases the recombination rate at the interfaces. These defects could behave as light sensitizing centers which have positive effect on the photoelectrical properties. What make the yttrium slab insertion worth of reporting is the remarkable enhancements that are achieved in the photosensitivity to laser light (406 nm), the larger return loss values that are achieved by the replacement of Yb by Y and the negative capacitance effect that is important for noise reduction in electronic circuits.

2. Experimental details

The yttrium nanosheets are inserted between two layers of CdS via thermal evaporation technique with the help of Norm-VCM 600 thermal vacuum evaporator. Chemically and ultrasonically treated glass substrates are used as transparent materials to grow the films. The evaporation cycles included 500 nm thick CdS films coated with 70 nm yttrium film. The produced CdS/Y films are re-coated with another

500 nm thick CdS films. All the films were prepared at substrate temperature of 25 ^{o}C. The temperature of the source was kept above 1100 ^{o}C [9] to guarantee stable formation of CdS. The evaporation rate of CdS was ~40 Å/s. Low evaporation rates ~10 Å/s is experimentally observed to form Cd_2S_3 phase. The reason for selecting the 500 nm value of CdS thickness is the experience in its technological applicability [4, 10]. Previously we succeed in fabricating tunneling diodes and dual band stop filters from 500 nm thick CdS films. The reason for selecting the value 70 nm thick is to prevent clustered formation of Y layers and to guarantee continues film formation. Yttrium films are known to exhibit amorphous nature and cause intermixing when sandwiched between two layers. The crystalline phase of Y films is observed above 60 nm [11]. The layers thicknesses were monitored by an in situ Inficon STM-2 thickness monitor connected to the quartz crystal inside the vacuum chamber. The monitor is capable of recoding 3000 data per second and has the resolution of 0.037 Å. The thickness monitor was calibrated based on sample thickness measured by interferometry technique.

Cu Kα radiation Miniflex 600 X-ray unit and COXEM 200 scanning electron microscope (SEM) equipped with EDAX energy dispersive X-ray spectrometer (EDS) are used to collect the structural, morphological and compositional information, respectively. The SEM unit can record images with variable accelerating voltages in the range of 5-30 kV. The EDS unit cover wide range of elements from carbon to nobelium. It operate in the range of 5-30 kV. The optical measurements including the transmittance and reflectance are carried out with the help of Evolution 300 spectrophotometer. The data were collected in the spectral range of 300-1100 nm. The photocurrent-power curves are collected with the Keithley current-voltage characteristics system. The system uses Keithley 235 voltage source and 6481 picoammeter attached through IEEE-488 to collect the data through MATLAB based software package. The light is irradiated from Thorlab laser source of a wavelength of 406 nm. The laser power is altered in the range of 0.01-6.0 mW. The impedance spectroscopy is measured by Agilent 4291B 1.0M–1.8 GHz impedance analyzer. The impedance analyzer is equipped with dielectric test fixture.

3. Results and discussion

The results of the X-ray diffraction (XRD) patterns for CdS and CdS/Y/CdS thin films are presented in Fig. 1 (a). It is clear from the figure that both of the CdS and CdS/Y/CdS thin films are of polycrystalline nature. The analysis of the X-ray diffraction patterns in accordance with "TREOR 92" and "CrystDiff" software packages reveal hexagonal type of structure. The lattice parameters (a and c) for CdS films are determined with the help of the equation, $d_{hkl}^{-2} = \frac{4}{3}(\frac{h^2+k^2+hk}{a^2})+\frac{l^2}{c^2}$. The equation takes into account, the observed interplanner spacing (d_{hkl}) between planes oriented in the (hkl) direction. The analysis of the reflection peaks which are shown in Fig. 1 indicated that the a and c values for double layers of CdS are 3.510 and 6.575 Å , respectively. The insertion of 70 nm thick yttrium between the two layers make the material exhibit lattice parameters of values of 3.558 and 6.672 Å, respectively. The Miller indices of the observed peaks which are shown in Fig. 1 (a) and the calculated lattice parameters, are consistent with the JCPDS # 067776 and also consistent with literature data [8, 12]. As the inset of Fig.1 (a) also illustrates, the maximum peak which is observed at 27.1^o shifts to 26.7^o. In addition, the maximum peak intensity increased from 1200 to 3200 a.u upon sandwiching of CdS with yttrium. It is evident from these numerical data that the presence of the yttrium slab between the two layers of CdS caused strained nature of growth. The calculated grain size (D), microstrain (ϵ), defect density and stacking faults using the previously described equations [13] revealed values of 34 nm, 4.35× 10^{-3}, 4.62× 10^{12} $lines/cm^2$ and 0.225%, respectively, for CdS thin films. These values shift to 28 nm, 5.52 × 10^{-3}, 6.77× 10^{12} $lines/cm^2$ and 0.272%, respectively, for CdS/Y/CdS. In contrast to what we have previously observed for CdS films sandwiched with ytterbium [8], the presence of yttrium slabs of thickness of 70 nm increased the lattice constant, defect density, microstrain, stacking faults and decreased the grain sizes in the CdS thin films. Such behavior could have raised from the differences in the ionic radiuses of Yb (87 pm [8]) and Y (102 pm [14]). Copper doped CdS thin films are also observed to exhibit hexagonal structure. Consistent with our observation,

the intensity of the reflection peak which is oriented in the (002) direction increased with increasing Cu content [12]. The behavior was assigned to the change in the scattering factor corresponding to the incorporated element. The participation of Yb and Cu in the structure of CdS increased the grain size and reduced the other structural parameters. These enhancements in the structural parameters which are not observed here were assigned to the Cd/Cu atomic ratio in Cu doped CdS [12] and to the recovery and recrystallization processes in CdS/Yb/CdS films [8].

For the purpose of observation of the morphology, the scanning electron microscopy images for the studied films are recorded and displayed in Fig. 1 (b) and its inset. For an enlargement of 60,000 times, very dense spherically shaped grains are observed. The samples surfaces are homogeneous. The average grain size for the CdS double layered films is 28 nm and for CdS/Y/CdS is 22 nm. The CdS/Y/CdS sample also included regions which are crowed with spherical grains of size of 28 nm. The results of the SEM analysis are close to that of XRD.

To investigate the atomic content in the currently studied samples (CdS/Y/CdS), dispersive energy X-ray spectroscopy (EDS) are carried out with the help of EDAX system attached to the electron microscope. During measurements, the standards used were, SiO_2 for Si and O, albite for Na, MgO for Mg, FeS_2 for S, wollastonite for Ca, yttrium for Y and cadmium for Cd. The accelerating voltage was 15 kV, the spot size was 12, more than 10 spots and three areas were analyzed at a counting time of 100-300 sec for each sample. The EDS spectra for the CdS/Y/CdS film are displayed In Fig. 2 (c). The spectrum is calculated for the area which is shown as inset-1of Fig. 1 (c). Most of the observed peaks correspond to the glass. The atomic distribution of the studied double layered CdS sample is found to be 53.38 at.% sulfur and 46.62 at. % Cd. For the CdS/Y/CdS sample, the atomic distribution (Shown in Fig. 1 (c)) is found to be 42.03 at.% Cd, 7.64% Y and 50.33% S. The numerical data suggests that a substitutional process has occurred during the growth and nucleation processes. Since the ionic

radius of Cd^{+2} is 96 pm [8] and that of Y^{+3} is 102 pm [14], replacement of Cd^{+2} by Y^{+3} is associated with stress that causes extension in the lattice parameters, compressing strain and also causes reduction of the grain size owing to the internal energy redistribution over the grains. The decrease in the grain size that is associated with increased defect density was also observed for Zn doped CdS thin films [15]. For these films, the shrinkage in the grain size was assigned as a reason for the increase in defect density. It is mentioned that the small grain size may generate large surface area which can form a large grain boundary surface areas. The grain boundary may be regarded as a crystal structural defect that affects or delays the transition of charge carriers [15].Literature data also reported information about the structural parameters of CdS thin films which are grown onto pristine and annealed at temperatures of 150, 300 and 450 ^{o}C [7]. It is mentioned that the lattice constant decreases upon annealing as a result of increased defects that arises from stress in the grains which take place during the treatment process [7]. The heat treatment increased the grain size due to the strong interactions between the vapor atom and substrates.

The difference in the behavior of the structural parameters upon replacement of Yb [8] with Y – metallic slabs in the current study may have raised from the crystalline nature of the metal slabs. While the Yb is known to exhibit face centered cubic structure with lattice parameters of $a = b = c =$ 5.487 Å [8], the yttrium is hexagonal structured metal with lattice parameters of $a = 3.6475$ and $c =$ 5.730 Å [16]. The hexagonal nature of structure of yttrium is confirmed from the XRD patterns which are also shown in figure 1 (a) for a yttrium thin film of thickness of 500 nm. The analysis of the XRD patterns of the yttrium films reveal hexagonal structure with lattice parameters of $a = 3.373$ and $c =$ 5.952 Å. The deviation of the lattice parameters for the Y thin film from the bulk values is assigned to the two dimensional nature of growth in addition to the substrate it is deposited onto. For the thin film of thickness of 70 nm, no strong reflection peak was detected. The absence of strong reflections is probability due to the stronger reflection of the glass substrates compared to the 70 nm thick Y.

Returning to the stoichiometry of the composition which revealed the empirical formula $Cd_{42.03}Y_{7.64}S_{50.33}$. The substitution of Y in sites of Cd causes the formation of Y-S bonds in the lattice of CdS. This may lead to the formation of Y_2S_3 as minor phase in the structure of CdS. The Y_2S_3 is a monoclinic system that has lattice parameters of values of $a = 17.523$ Å, $b = 4.011$ Å, $c = 10.174$ Å and $\beta = 98.601^o$ (COD 4030478). Such phase if formed would cause large strain on the unit cells of CdS which in turn lead to larger defects values as we observed in this work. The inability of the X-ray diffraction technique to detect this minor phase arises from it is amount which should be less than 10% of the total volume.

The effects of yttrium on the optical performance of CdS are illustrated in Fig.2. The measured transmittance (T) and reflectance (R) spectra are shown in Fig. 2 (a) and (b), respectively. It is clear from the transmittance spectra that the effect of yttrium thin slabs become effective for incident light wavelength (λ) larger than 508 nm. For all $\lambda < 508\ nm$, the trend of variation of the CdS/Y/CdS is the same as that of CdS double layers. For all $\lambda > 508\ nm$, the transmittance spectra redshifts. On the other hand, the reflectance spectra which are presented in Fig. 2 (b) exhibit increased values of *R* and a redshift in the maximum peak. Particularly, the peak which appeared at 536 nm (2.32 eV) in the reflectance spectra of CdS shifts to 552 nm (2.25 eV) upon insertion of yttrium slabs between two layers of CdS. The total effect which is readable from the absorption coefficient (α) spectra are displayed in Fig. 2 (c). The α-spectra which is calculated by the previously described methods [8] exhibits four regions of absorption. The high energy region (4.1-2.93 eV) where the α-spectra appears to be saturated due to the generation of carriers resulting in nonlinear renormalization of the band gap with increasing electromagnetic field intensity [17] or due to exciton resonance at these levels [17]. The second region is the strong absorption region (2.92-2.24 eV). In this region, as both samples exhibit the same value, no effect of the yttrium slabs is observed. The third region is the weak absorption region (2.23-1.39 eV). In this region a clear redshift in the α −spectra can be observed. In the fourth region (1.38-1.14 eV), α −spectra show increasing trends of variation with decreasing

incident light energy. Such behavior is usually assigned to the free carrier absorption. The free carrier absorption happens as a result of the carrier movement which is induced by phonon scattering. The phonon scattering transfers energy to lattice when irradiated by IR light [18].

The enhancement of the absorbability in the CdS via yttrium slab insertion can be guessed from the absorption coefficients ratio ($R_\lambda = \frac{\alpha_{CdS/Y/CdS}}{\alpha_{CdS}}$; R_λ absorbability). The absorbability spectra is illustrated in the inset of Fig. 2 (c). It is clear from the figure that the absorbability region of the CdS/Y/CdS extends from 2.40 to 1.28 eV. It exhibits maxima at 1.73 eV. The presence of Y between two layers of CdS increased the absorbability by 5 times in the visible and IR region. Such property makes the Y sandwiched CdS more appropriate for optoelectronic applications as it enhances the optoelectronic properties of this material. The values of R_λ are comparable to those we previously observed for CdS/Yb/CdS structure. For this structure a R_λ value of 7.8 was detected at 1.64 eV [8].

Fig. 3 (a) and (b) illustrates the Tauc equation plotting for the absorption coefficient spectra in the sharp (second) and weak absorption (third) regions, respectively. The plotting of $(\alpha E)^2 - E$ variation which is shown in Fig. 3 (a) was linear only in the region of strong absorption. The E −axis crossing in that region reveal energy band gaps of values of 2.42 and 2.44 eV for the CdS and CdS/Y/CdS films, respectively. No significant role of the Y-slab in this region is observable as the difference in the energy band gap values is within the experimental error which is ~2% of the measured value. The reason for the less effect of the Y-slab on the direct allowed transitions in CdS is unknown but probably assigned to the restrictions of the spin-orbit coupling and quantum mechanical selection rules. The direct allowed transition energy band gap is the same as that we previously observed for CdS [8]. The effect of the Y-participation in the structure of CdS becomes pronounced when the indirect allowed transition energy band gap is taken into account. The plotting of the $(\alpha E)^{\frac{1}{2}} - E$ variation in the weak absorption regions (third region) which are presented in Fig. 3 (b) reveal an indirect allowed transitions energy band gap of values of 1.50 and 1.14 eV for CdS and CdS/Y/CdS films, respectively. Remarkable redshift from 1.50 to 1.14 is observed upon Y-participation. The band gap difference is

0.36 eV. The indirect allowed transitions energy band gap being 1.50 eV was previously observed for CdS thin films prepared by the chemical bath deposition technique [19]. The redshift in the indirect allowed energy band gap upon Y-slab insertion could be assigned to the increase in the lattice parameters, increase in the microstrain and increase in the defect density as we have discussed in the structural analysis. In addition to the structural reasons, the electronic configuration point of view is also worth of consideration. Particularly, since the electronic configuration of Y^{39} is $4d^1 5s^2$ and that of Cd^{48} is $4d^{10}5s^2$, Y^{39} comprise empty states in it is $4d-$orbitals. These states can behave as conduction bands as they accept electrons. The overlapping of the energy levels in the $4d-$orbitals of Y and Cd make it easier for electrons to transfer to a closer energy level which is available by the presence of yttrium [8]. For Cu doped CdS thin films, the shrinkage in the energy band gap of CdS upon copper doping was assigned to creation of traps within the band gap that may cause formation of the states near the band edge leading to the observed band gap shrinkage [20].

Fig. 3 (c) display the real part (ε_r) of the dielectric constant being calculated with the previously described methods [8]. An important feature of the dielectric spectra appears in the spectral range of 3.5-1.14 eV. Although the dielectric spectra of CdS/Y/CdS exhibit the same shape like that of double layers of CdS, there is a redshift in the position of maximum peak. Particularly, while the CdS exhibit a resonance peak of ε_r of value of 9.13 at 2.27 eV, the yttrium slabs shifted the peak to 2.17 eV and increased the dielectric constant value to 12.39. It indicates an enhancement of 35.7% in the dielectric constant value. The presence of the dielectric resonance at 2.27 eV was assigned to the transition between the valance and conduction band being associated with recombination processes as a result of second ionization of sulfur vacancies [8, 21]. The redshift in the dielectric spectra could be assigned to change in the recombination mechanism as a result of presence of yttrium which is observed to increase the defect density on the surface of CdS films.

As practical application to the current design, the photocurrent (I_{ph}) was recorded as function of laser power (P). A laser light of wavelength of 406 nm was used to irradiate the samples surfaces. The

resulting photocurrent-power curves are presented in Fig. 3 (d). The figure shows remarkable enhancement in the photocurrent values due to the insertion of yttrium between two layers of CdS. Namely, at particular power 6.0 mW, for example, the photocurrent of double layers CdS exhibit value of 30 nA. The photocurrent value increases to 631 nA when the CdS/Y/CdS was irradiated with the same power of laser light. An enhancement of 21 times is achieved by the this technique. These numerical values make the replacement of the ytterbium by yttrium preferable as the Yb slab inserstion increases the photocurrent value to 190 nA resulting in enhancement of photosensitivity by 6.3 times only. On the other hand, one may observe a difference in the slopes of the $\ln(I_{ph}) - \ln(P)$ dependencies. A logarithmic plot of the power dependent photocurrent in accordance with the rule, $I_{ph} = I_{ph0}P^{\gamma}$, reveal γ value of 0.65 for double layered CdS and γ value of 1.34 and 0.49 for CdS/Y/CdS and CdS/Yb/CdS films, respectively. The standard values of γ for linear and sublinear recombination mechanisms are 1.0 and 0.5, respectively. While $\gamma > 1.0$ means there is strong electron-hole recombination at the surface, any γ value between 1.0 and 0.50 indicate that the recombination is associated with exponential traps distribution [22, 23]. The presence of traps in the double layered CdS films could be due to the Cd vacancies. The compositional analysis revealed 53.38 at.% sulfur and 46.62 at. % Cd. Thus, the change in the recombination mechanism from traps assisted sublinear ($\gamma = 0.65$) and from sublinear in the presence of Yb nanolayer to supralinear is due to the Y filling in vacant sites of Cd. This belief is supported by the EDS results which indicate that the atomic sum of Cd and Y is 49.67% and that of S is 50.33%. Another reason that is worth of consideration is the increased defect density on the surface of the CdS/Y/CdS as a result of strained nature of growth. The defects behave as sensitizing centers which convert from traps to recombination centers under strong light irradiation [22, 23].

To find another application for the CdS/Y/CdS films, we have followed our previous procedure which we used for CdS/Yb/CdS [8] films. Namely, The CdS/Y/CdS films were deposited onto Yb substrate and coated with Au (point contacts of area of $7.8\times 10^{-3}\ cm^2$). The Yb metal is selected because it

has low work function (2.51 eV [24]) and the Au is selected owing to its high work function (5.34 eV) [24]. As the CdS and CdS/Y/CdS films exhibit *n*-type conductivity and the work function of CdS and CdS/Y/CdS are less than 4.7 eV [4], The Au forms a Schottky type of contact at the Au side and an ohmic metal-semiconductor interface is formed at the Yb side. The response of these devices to ac signals of amplitude of V=0.10 V is screened in the frequency domain of 10-1800 MHz. Remarkable enhancement in the performance of the Yb/CdS/CdS/Au device is observed from the capacitance spectra. The capacitance spectra for the Yb/CdS/Y/CdS/Au device which is illustrated in Fig. 4 (a), show negative capacitance effect in the frequency domain of 450-1800 MHz. It exhibits very narrow peak at 460 MHz. This effect is not observed for the Yb/CdS/CdS/Au device nor it is observed in CdS/Yb/CdS films [8] (additionally illustrated as brown colored in Fig.4 (a)). Negative capacitance is important property of Schottky type devices as it indicates the applicability of these types of devices in integrated circuits for parasitic capacitance cancellation [4, 25]. It plays vital role in noise reduction in power circuits. Negative capacitance effect is usually assigned to the to the non-equilibrium interfacial states that forces electrons to hope from interfacial to the bulk states. It could also be attributed to the surface and bulk trap states as we observed from the photocurrent-light power analysis [4, 25].

As practical application of the proposed devices in microwaves filtering we observe the deference between the impedance (Z) spectra of both devices. The impedance spectra is shown in Fig. 4 (b). while the Z values decreased by four decades, upon increasing the frequency from 10 to 1800 MHz, that of Yb/CdS/Y/CdS/Au remain constant in the range of 10-100 MHz. It, then, slowly decreases reaching minimum value at 460 MHz and then re-increases with increasing signal frequency. The main difference between the impedances of the CdS/Y/CdS and CdS/Yb/CdS is presented by the numerical value. Particularly, while yttrium causes CdS to exhibit low impedance spectra, the Yb forces high impedance. The total impedance effect on microwave signals is better read from the magnitude of the reflection coefficient ($\rho=\frac{Z_{sample}-Z_{source}}{Z_{sample}+Z_{source}}$) spectra. The ρ spectra are shown in Fig. 4 (c). While ρ value

is always 1.0 for the Yb/CdS/CdS/Au device which indicate an open load with no match between device and source, the Yb/CdS/Y/CdS/Au device show good performance as band stop filter. The device behaves as high pass filter in the frequency domain of 10-300 MHz, low pass filters in the domain of 300-1520 MHz and band stop filter in the domain of 300-1800 MHz with notch frequency of 1520 MHz. The performance of Yb/CdS/Au/CdS/Au device is much better than that sandwiched with Yb (shown by brown color in Fig. 4 (c)). The quality of this signal is detected from the return loss ($L_r = -20\log(\rho)$). Return loss in communication engineering refers to the loss of power in the signal rejected by a discontinuity in devices under test. It is a measure of how well devices are matched. A match is good if the return loss is high ($L_r > 20\ dB$). The return loss spectra of the Yb/CdS/Y/CdS/Au device are shown in Fig. 4 (d). It reaches value of 35 dB at 1520 MHz. It suggests that the device is ideal for use as band stop filters of notch frequency of 1520 MHz. The main difference between the CdS/Yb/CdS and CdS/Y/CdS is that the yttrium exhibit higher return loss values compared to Yb which reveal L_r value of 22.6 dB at 1.35 GHz [8]. Both metals provide the CdS films with the property of microwaves filtering. Without metal sandwiching, the Yb/CdS/CdS/Au device exhibit very poor features for waves trapping in the microwave region. The shift in the notch frequency value from 1350 to 1520 MHz upon replacement of Yb with Y can be ascribed to the structural modifications that controlled the capacitance and resistance values. The microwave cavity's resonance frequency is usually controlled by the values of capacitance and resistance.

As a complementary work to the previously published data [8] we have calculated the optical conductivity from the imaginary part of the dielectric constant ($\sigma(w) = \varepsilon_{im}\frac{w}{4\pi}$, w: angular frequency) and computed the optical conductivity parameters with the help of Drude - Lorentz models using the equation (Eqn. 1) given in reference 5. The optical conductivity spectra which are shown in Fig. 5 follow the same trend of variation like that we reported for CdS/CdS and CdS/Yb/CdS thin films. However, the computed optical parameters which reproduce the experimental data (black circles in Fig. 5) are somehow different. Particularly, comparing the data of Table 1 which is reported here with

the previously reported [8] optical conductivity parameters for CdS/CdS and CdS/Yb/CdS thin films, one may observe significant difference between the optical conductivity parameters of the first and second oscillators (*i=1, 2*). As for example, the scattering time (τ_1) increased from 4.0 to 30 fs and the free carrier density (n_1) decreased from $4.0 \times 10^{17}\ cm^{-3}$ to $1.2 \times 10^{17}\ cm^{-3}$ upon insertion of Y between two layers of CdS. The plasmon frequency (W_{pe1}) decreased from 0.84 GHz [8] to 0.62 GHz and the reduced resonant frequency (W_{e1}) did not change upon sandwiching of Y between two layers of CdS. The drift mobility (μ_{e1}) of two stacked layers of CdS which exhibited value of 281.3 cm^2/Vs for CdS thin films increased to 475 cm^2/Vs for the CdS/Y/CdS samples. These values are very close to the literature data were a value of 500 cm^2/Vs is reported [26, 27]. Even though the drift mobility is remarkably increased via insertion of the hexagonal yttrium between two stacked layers of hexagonal CdS, still the respective values of mobility, plasmon frequency and free carrier density are higher for the CdS/Yb/CdS than those of CdS/Y/CdS films. We believe that the main reason for the higher absorbability values of CdS/Yb/CdS compared to CdS/Y/CdS and the better effects on optical performance of Yb over Y –sandwiched films mostly lay in the electronic configuration of the metals. Yb ($4f^{14}6s^2$) is better than Y ($4d^15s^2$) due to the overlapping of the f states with Cd ($4d^{10}5s^2$) and S ($3s^23p^4$) atomic orbitals as the *f* state is at higher energy than those of d orbitals. In addition the lack of nine electrons from $4d$ orbital states of Y makes electron transitions from $4d$ orbitals of Cd to Y possible. The orbital sharing of electrons of Cd ($4d^{10}5s^2$) with empty *d* orbitals of Y ($4d^15s^2$) that is accompanied with less lattice mismatches and the presence of f orbitals in Yb could be reasoning for the better performance of Yb as an optical conductor over that of Y. However, the achievements presented by the negative capacitance effect, higher return loss values and higher photosensitivity to laser light make the CdS/Y/CdS worthy of consideration.

It is also worth mentioning that the optical conductivity parameters presented by the drift mobility value for the CdS/Y/CdS or CdS/Yb/CdS are much higher than those we reported for other sandwiched systems like Ga_2S_3/In/Ga_2S_3 (GIG) [28]. For this system the maximum drift mobility of value of 12.58

cm^2/Vs was observed. It is also much higher than those which are reported for CuSe/Yb/CuSe as 35.2 cm^2/Vs [29]. The high values of the drift mobility with the continuously increasing optical conductivity with increasing incident photon energy make the CdS thin films preferable for thin film transistor technology which acquire fast response and mobile charge carrier transport.

4. Conclusions

In the current study we have investigated the effects of insertion of yttrium between two layers of CdS on the physical properties of CdS thin films. The yttrium atoms substituted sites of Cd causing compressing strain that in turn decreased the grain size and increased the microstrain and defect density values. Optically, the absorbability of the CdS increased upon Y-participation. The increased absorbability is associated with enhanced photoconductive response and improved dielectric property. On the other hand, the electrical analysis revealed the suitability of the CdS/Y/CdS device for use as band stop filters of notch frequency of 1520 MHz.

Acknowledgments

This project was funded by the Deanship of Scientific Research (DSR) at the Arab American University, Palestine (AAUP). The authors, therefore, acknowledge with thanks the DSR and the AAUP technical and financial support.

References

[1] B. Gao, Y. Zhao, L. Cai, P. Liu, Z. Liang, and H. Shen, Fabrication of cadmium sulfide/p type silicon heterojunction solar cells under 300° C with more than 10% efficiency, Solar Energy 173 (2018) 635-639.

[2] F. Zhang, H.-Q. Zhuang, J. Song, Y.-L. Men, Y.-X. Pan and S.-H. Yu, Coupling cobalt sulfide nanosheets with cadmium sulfide nanoparticles for highly efficient visible-light-driven photocatalysis, Applied Catalysis B Environmental 226 (2018) 103-110.

[3] S. Zhang and Y. Kuo, Memory Functions of Cadmium Sulfide Embedded Zr-Doped HfO2 High-k Dielectrics, ECS Journal of Solid State Science and Technology 7, no. 5 (2018) Q97-Q103.

[4] N. M. Khusayfan, A. F. Qasrawi, and H. K. Khanfar, Design and electrical performance of CdS/Sb_2Te_3 tunneling heterojunction devices, Materials Research Express 5, no. 2 (2018) 026303.

[5] Chander, Subhash, and M. S. Dhaka. "Optimization of substrates and physical properties of CdS thin films for perovskite solar cell applications." *Journal of Materials Science: Materials in Electronics* 28, no. 9 (2017): 6852-6859.

[6] Chander, Subhash, and M. S. Dhaka. "Optical and structural constants of CdS thin films grown by electron beam vacuum evaporation for solar cells." *Thin Solid Films* 638 (2017): 179-188.

[7] Purohit, Anuradha, S. Chander, and M. S. Dhaka. "Thermal evolution of physical properties of evaporated CdS thin films for perovskite solar cell applications." *Vacuum* 153 (2018): 35-38.

[8] T. Y. Abed, A. F. Qasrawi, and S. E. Al Garni, Investigation of the physical properties of the Yb nanosandwiched CdS films, Journal of Alloys and Compounds 731 (2018) 1022-1028.

[9] V. Ruxandra and S. Antohe. The effect of the electron irradiation on the electrical properties of thin polycrystalline CdS layers, Journal of applied physics 84 (1998) 727-733.

[10] H. K. Khanfar, A. F. Qasrawi, and S. R. Shehada, Negative Capacitance Effect in Ag/α-In 2 Se 3/CdS/CdSe/C Dual Band Stop Filters, Journal of Electronic Materials 48 1 (2019) 244-251

[11] T. L. Lee, and L. J. Chen, Formation of amorphous interlayers in ultrahigh vacuum deposited yttrium thin films on (111) Si, Journal of applied physics 73 (1993) 5280-5282.

[12] P. Reyes, and S. Velumani, Structural and optical characterization of mechanochemically synthesized copper doped CdS nanopowders, Materials Science and Engineering B 177, no. 16 (2012) 1452-1459.

[13] A. Omar, A. F. Qasrawi, and N. M. Gasanly, Temperature effects on the structural and optical properties of the TlInSe2xS2 (1− x) mixed crystals (x= 0.3), Journal of Alloys and Compounds 724 (2017) 98-102.

[14] M. Maczka, and P. Pasierb, Synthesis and properties of barium modified yttrium borate, Materials Research Bulletin87 (2017) 84-91.

[15] A. A. Ibiyemi, A. O. Awodugba, O. Akinrinola, and A. A. Faremi, Zinc-doped CdS nanoparticles synthesized by microwave-assisted deposition, Journal of Semiconductors 38, no. 9 (2017) 093002.

[16] E. Kooij, S. Ernst, J. H. Rector, D. G. Nagengast, J. W. J. Kerssemakers, B. Dam, R. Griessen, A. Remhof, and H. Zabel, Growth and hydrogenation of epitaxial yttrium switchable mirrors on CaF2, Thin solid films 402, no. 1-2 (2002) 131-142.

[17] Ch. M. Bowden, C. C. Sung, J. W. Haus, and J. M. Cook, Longitudinal spatial inhomogeneities in intrinsic optical bistability due to induced absorption, JOSA B5, no. 1 (1988) 11-19.

[18] J. Lai, J. Zhang, Y. Mao, L. Lin, J. Min, X. Liang, J. Huang, K. Tang, and L. Wang, Distribution of Te Inclusions in CdMnTe Crystal Grown by Traveling Heater Method, J. Electron. Mater. 47 (2018) 4219-4255

[19] A. Kariper, E. Güneri, F. Göde, C. Gümüş, and T. Özpozan, The structural, electrical and optical properties of CdS thin films as a function of pH, Materials Chemistry and Physics129, no. 1-2 (2011) 183-188.

[20] A. A. Ziabari, and F. E. Ghodsi, Influence of Cu doping and post-heat treatment on the microstructure, optical properties and photoluminescence features of sol–gel derived nanostructured CdS thin films, Journal of Luminescence 141 (2013) 121-129.

[21] K.E. Nieto-Zepeda, A. G._En-Cervantes, K. Rodríguez-Rosales, J. Santos-Cruz, D. Santos-Cruz, M.D.L.L. Olvera, O. Zelaya-_Angel, J. Santoyo-Salazar, L.A. Hern_andez-Hern_andez, G. Contreras-Puente, F. de Moure-Flores, Effect of the sulfur and fluorine concentration on physical properties of CdS films grown by chemical bath deposition, Results Phys. 7 (2017) 1971-1975.

[22] R. H. Bube, Photoelectronic properties of semiconductors. Cambridge University Press, 1992.

[23] A. F. Qasrawi, T. S. Kayed, and İsmail Ercan, Photoconductivity kinetics in AgIn5S8 thin films, Journal of Alloys and Compounds 508, no. 2 (2010) 380-383.

[24] H. L. Skriver, and N. M. Rosengaard, Surface energy and work function of elemental metals, Physical Review B 46, no. 11 (1992) 7157.

[25] Sh. Wang, and F. C. Lee, Common-mode noise reduction for power factor correction circuit with parasitic capacitance cancellation, IEEE Transactions on Electromagnetic Compatibility 49, no. 3 (2007) 537-542.

[26] S. Antohe, L. Ion, and V. A. Antohe. The effect of the electron irradiation on the structural and electrical properties of $A^{II}B^{VI}$ thin polycrystalline films, Journal of Optoelectronics and Advanced Materials 5 (2003) 801-816.

[27] O. Toma, R. Pascu, M. Dinescu, C. Besleaga, T. L. Mitran, N. Scarisoreanu, and S. Antohe. Growth and characterization of nanocrystalline CdS thin films, Chalcogenide Letters 8 (2011) 541-548.

[28] E. O. Nazzal, A. F. Qasrawi, and S. R. Alharbi, Engineering the Optical and Dielectric Properties of the Ga 2 S 3/In/Ga 2 S 3 Nanosandwiches via Indium Layer Thickness, Plasmonics 13, no. 3 (2018) 1049-1056.

[29] N. M. Khusayfan, and H. K. Khanfar. Structural and optical properties of Cu2Se/Yb/Cu2Se thin films, Results in Physics 12 3 (2019) 645-651.

List of Figure Captions

Fig. 1. (a) The X-ray diffraction patterns for yttrium, CdS and CdS/Y/CdS films, (b) the scanning electron microscopy images (SEM) for CdS/Y/CdS films and (c) The energy dispersive X-ray spectra (EDS) for CdS/Y/CdS films. The inset of (a) show the shift in the XRD main peak, inset of (b) show the SEM image for CdS and inset of (c) show the scanned area for the EDS test.

Fig. 2. (a) The transmittance, (b) the reflectance and (c) the absorption coefficient spectra for the CdS and CdS/Y/CdS films. The inset of (c) show the absorbability spectra.

Fig. 3. The Tauc equation plots in (a) the second and (b) third absorption region, (c) the dielectric spectra and (d) the photocurrent-power dependence for the CdS and CdS/Y/CdS thin films.

Fig. 4 (a) the capacitance, (b) the impedance, (c) the reflection coefficient and (d) the return loss spectra for the Yb/CdS/Au and Yb/CdS/Y/CdS/Au devices.

Fig. 5 The optical conductivity for CdS/Y/CdS samples. The dark circles represent the fitting of the optical conductivity with the help of the Drude-Lorentz model.

Table 1: The fitting parameters for CdS/Y/CdS nanosandwiched films in accordance with Drude-Lorentz model

	CdS/Y/CdS				
i	1	2	3	4	5
τ_i (fs)	30.00	1.00	0.75	0.60	0.70
W_{ei} (x10^{15} Hz)	1.6	3.2	4.2	5.2	6.2
n($\times 10^{17}$ cm^{-3})	1.2	2.0	8.50	13.0	14.0
μ (cm^2/Vs)	475	16	12	10	11
W_{pei} (GHz)	0.62	0.80	1.64	2.03	2.11

Research Highlights

- 70-nm yttrium layer inserted between two 500-nm CdS films
- Y increased the lattice parameters and formed a strained structure
- The optical absorbion is enhanced at 1.74 eV and the bandgap redshift
- The photosensitivity increased 21 times by the insertion of a Y interlayer
- CdS/Y/CdS film structures show negative capacitance and microwave filtering property.

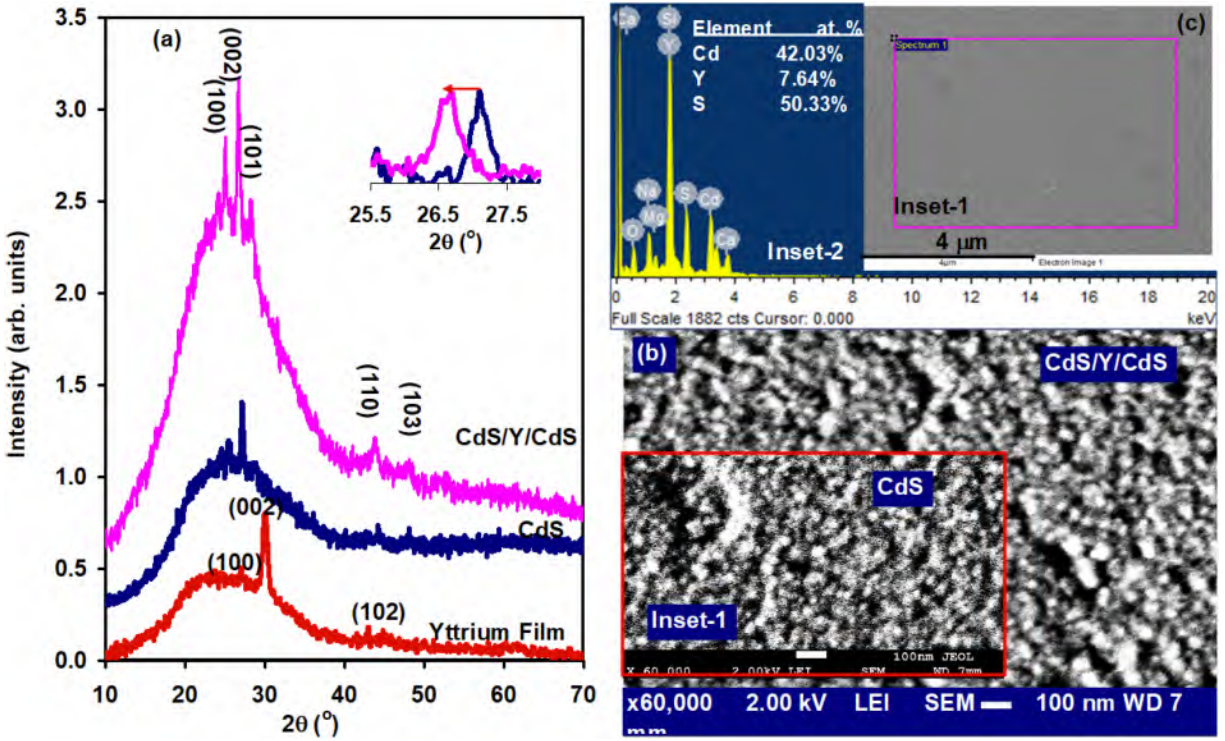
(a)
(002)
(100)
(101)
(110)
(103)
(102)
CdS/Y/CdS
CdS
Yttrium Film
Intensity (arb. units)
2θ (°)
25.5 26.5 27.5
2θ (°)
Element at. %
Cd 42.03%
Y 7.64%
S 50.33%
Inset-2
Full Scale 1882 cts Cursor: 0.000
keV
(c)
Inset-1
4 μm
(b)
CdS/Y/CdS
CdS
Inset-1
100nm JEOL
x60,000 2.00 kV LEI SEM 100 nm WD 7

Figure 1

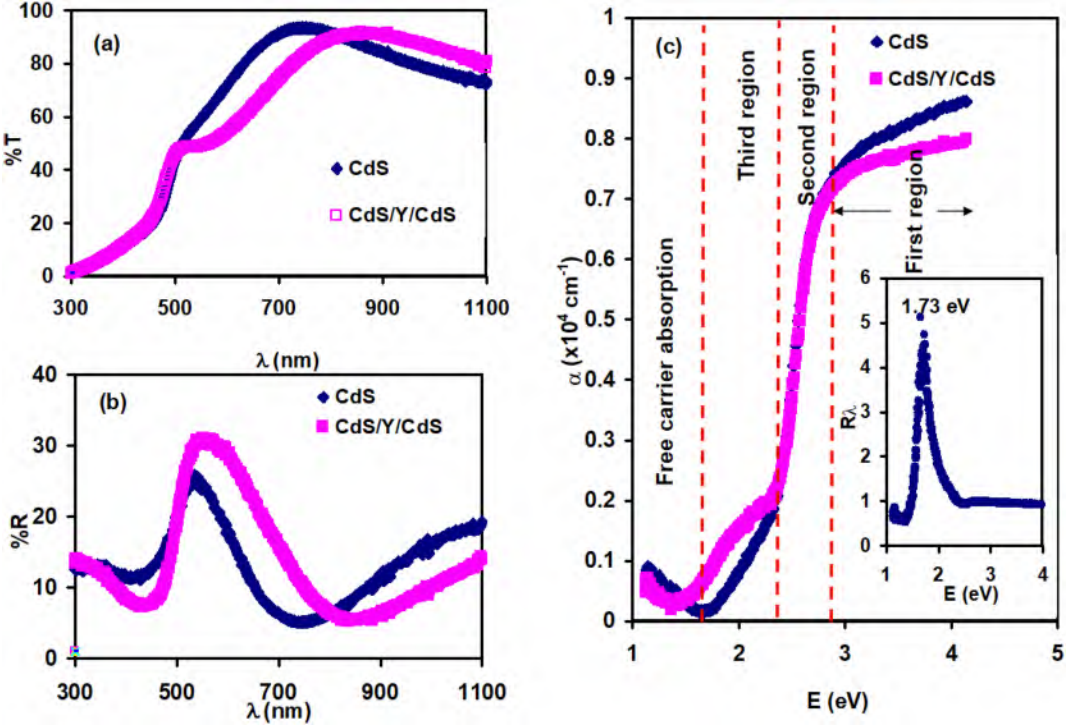
(a)
%T
CdS
CdS/Y/CdS
λ (nm)
(b)
%R
CdS
CdS/Y/CdS
λ (nm)
(c)
CdS
CdS/Y/CdS
Free carrier absorption
Third region
Second region
First region
α (x10⁴ cm⁻¹)
1.73 eV
Rλ
E (eV)
E (eV)

Figure 2

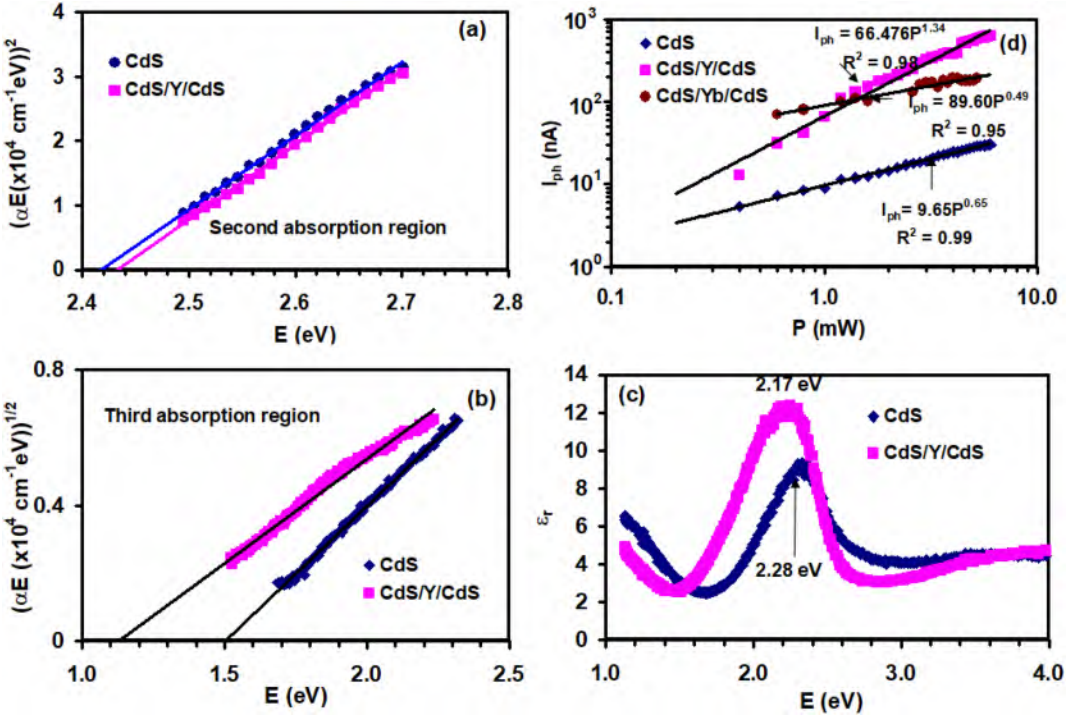
(a)
CdS
CdS/Y/CdS
Second absorption region
$(\alpha E(x10^4\ cm^{-1}eV))^2$
E (eV)
(b)
Third absorption region
CdS
CdS/Y/CdS
$(\alpha E\ (x10^4\ cm^{-1}eV))^{1/2}$
E (eV)
(d)
CdS
CdS/Y/CdS
CdS/Yb/CdS
$I_{ph} = 66.476P^{1.34}$
$R^2 = 0.98$
$I_{ph} = 89.60P^{0.49}$
$R^2 = 0.95$
$I_{ph} = 9.65P^{0.65}$
$R^2 = 0.99$
I_{ph} (nA)
P (mW)
(c)
2.17 eV
2.28 eV
CdS
CdS/Y/CdS
ε_r
E (eV)

Figure 3

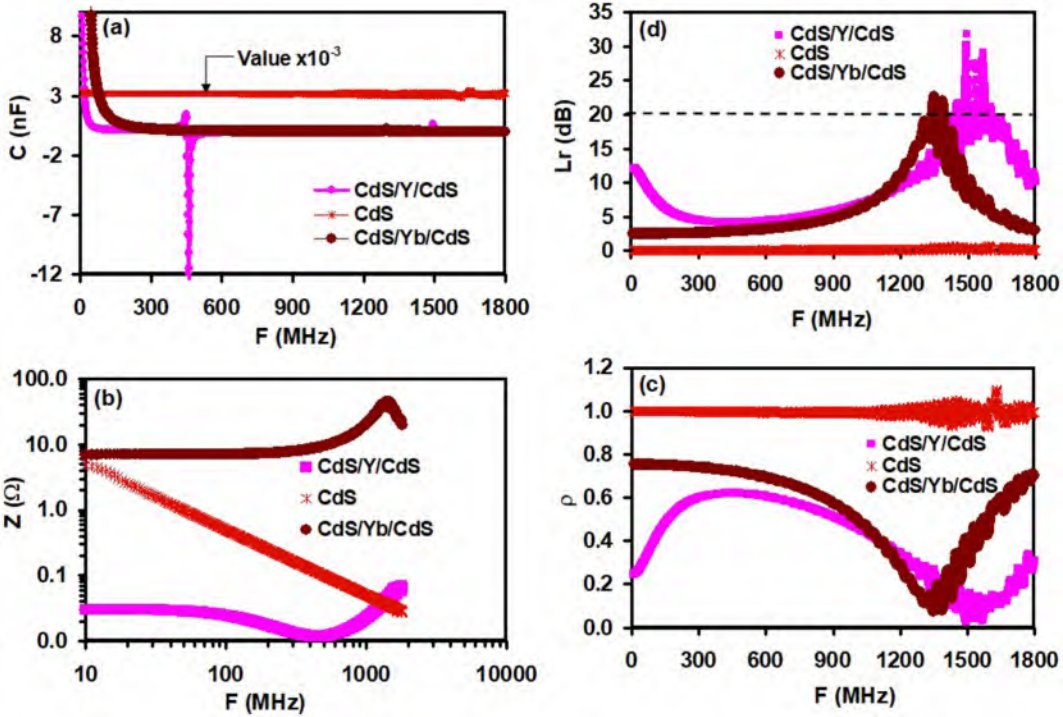
(a)
Value x10-3
C (nF)
F (MHz)
CdS/Y/CdS
CdS
CdS/Yb/CdS
(b)
Z (Ω)
F (MHz)
CdS/Y/CdS
CdS
CdS/Yb/CdS
(d)
Lr (dB)
F (MHz)
CdS/Y/CdS
CdS
CdS/Yb/CdS
(c)
ρ
F (MHz)
CdS/Y/CdS
CdS
CdS/Yb/CdS

Figure 4

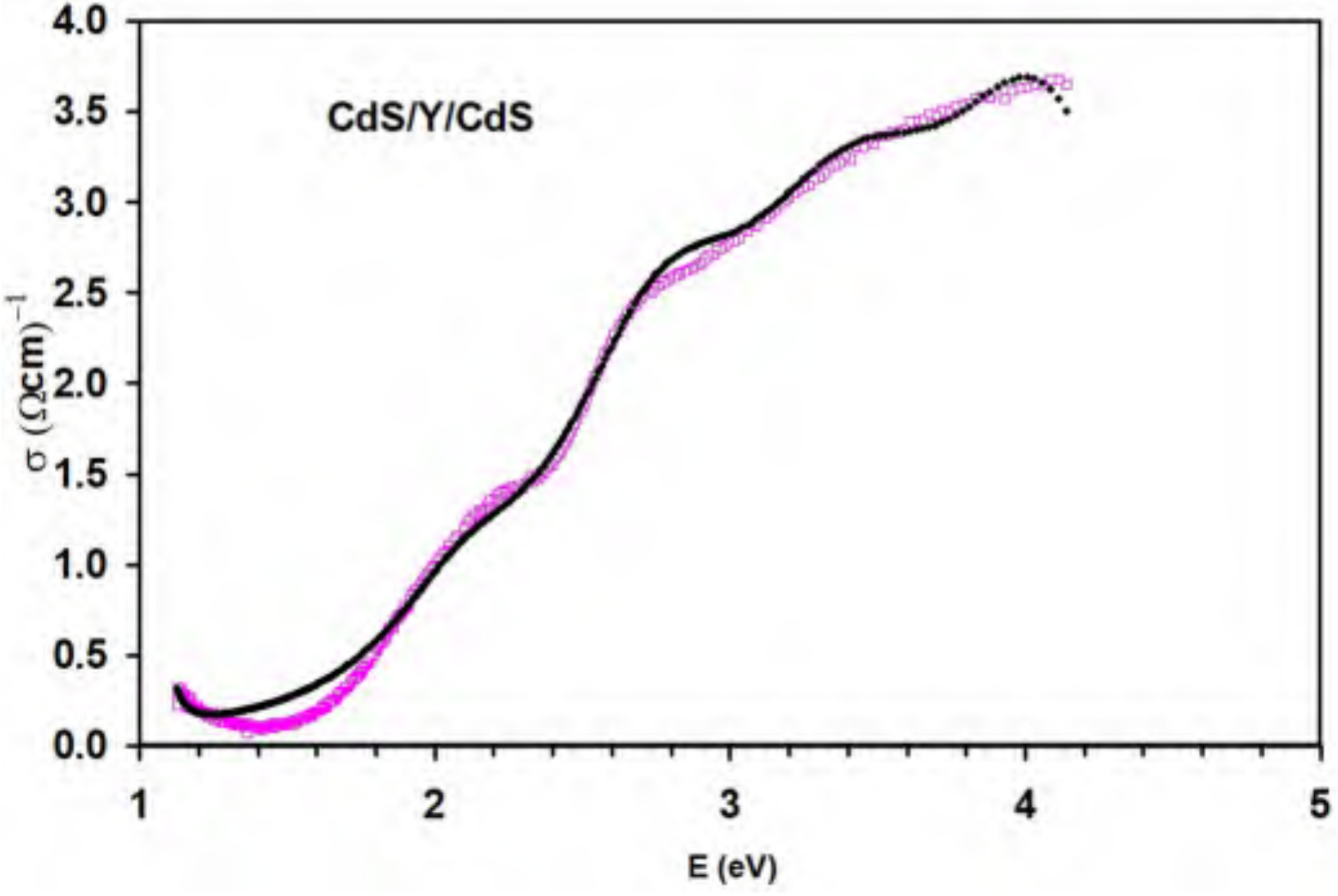

Figure 5